Electronic Supplementary Material (ESI) for Journal of Materials Chemistry C.

ESI

Chiral Toroids and Tendril Superstructures from Integrated Ternary Species with Consecutively Tunable Supramolecular Chirality and Circularly Polarized Luminescence

Zhaohui Zong,[a] Peng Zhang,[b] Hongwei Qiao,[c] Aiyou Hao*,[a] and Pengyao Xing*,[a]

[a]*School of Chemistry and Chemical Engineering, Shandong University, Jinan 250100, People's Republic of China. Email:haoay@sdu.edu.cn; xingpengyao@sdu.edu.cn*

[b]*Shandong Chengchuanglanhai Pharmaceutical Technology CO., LTD, 2350 Kaituo Road, Jinan, People's Republic of China.*

[c]*Shandong Shengquan New Material Co., Ltd, Jinan, People's Republic of China.*

Experimental section

Materials

All chemicals were purchased from Guoyao Chemical Reagent Co. Ltd, Shanghai, which were used without further purification. NS, PS and TBIB were synthesized according to the previous report.[S1]

Characterizations

Scanning electron microscope (SEM) images were attained by a Zeiss scanning electron microscope. The samples for SEM detection were dropped in the silicon pellet, dried and then sprayed by the gold. Transmission electron microscope (TEM) was measured on a JEM-100CX II electron microscope. The samples for TEM detection were dropped in the copper grid and air-dried. Powder X-ray diffraction (XRD) patterns were collected on a German Bruker/D8 Advanced diffractometer with Cu Kα radiation (λ = 0.15406 nm, voltage 40 KV, current 40 mA). The samples were casted onto cover glasses (18 mm × 18 mm) and dried to form thin films. AFM testing was conducted with a Veeco Nanoscope Multimode Ш SPM and operated in tapping contact mode at ambient temperature. The AFM sample was dropped on the mica wafer and dried. CD and CPL were collected with an Applied Photophysics ChirascanV100 model. CD spectra were collected in solution phase. As the colloidal self-assemblies may be inhomogeneous during measurement, we utilized vortex to further blend the self-assemblies before measurement and the cuvette with a length of 1 mm was used. Differently, CPL was carried out in thin film state. Self-assemblies were centrifuged to remove most of solvents, followed by drop casting on quartz plates to give homogenous thin films. To eliminate linear dichroism artifacts, rotation of the sample angle to the beam was applied, and no apparent artificial signal has been observed. Ultra-high-resolution CLSM was performed on a Leica TCS SP8. GiSWAXS was measured with a Xeuss 2.0 by Xenocs.

Self-assembly

Self-assembly was triggered by nanoprecipitation method. A solvent exchange protocol was applied. In detail, all building blocks were dissolved into DMSO as 100 mM stock solutions. By injecting certain volume stock solution (10 μl for instance) into bulky DI water (990 μl for instance), followed by aging at ambient conditions for at least 8 h before testing, a self-assembly system was achived (1 mM). Coassemblies were prepared utilizing same protocol.

Computational details

The native structures of building units comprising of *L*-PS, TCNB and TBIB were built from the GaussView06 program, which were initially optimized, and the electrostatic potential (ESP) was simultaneously calculated by Hartree-Fork method. The geometry optimized building units were built by Insert-Molecule modulus into columnar preassemblies comprising of 60 CT complexes (*L*-PS/TCNB) for binary system and 180 *L*-PS, 180 TCNB and 120 TBIB for the ternary system with a ~3.5 Å *d*-spacing. The water solvent simulated was the SPC216 model. The Antechamber program was used to fit the restrained electrostatic potential (RESP) charge, and then the general Amber force field (GAFF) was adopted to parameterize the for subsequent MD simulations. All MD simulations were implemented with the GROMACS 2020 program. Energy minimization was conducted using the steepest descent algorithm before performing dynamic simulations. MD simulations for system were carried out for 10 ns with a time step of 0.002 ps per integration step under the ensemble conditions of T = 298 K.

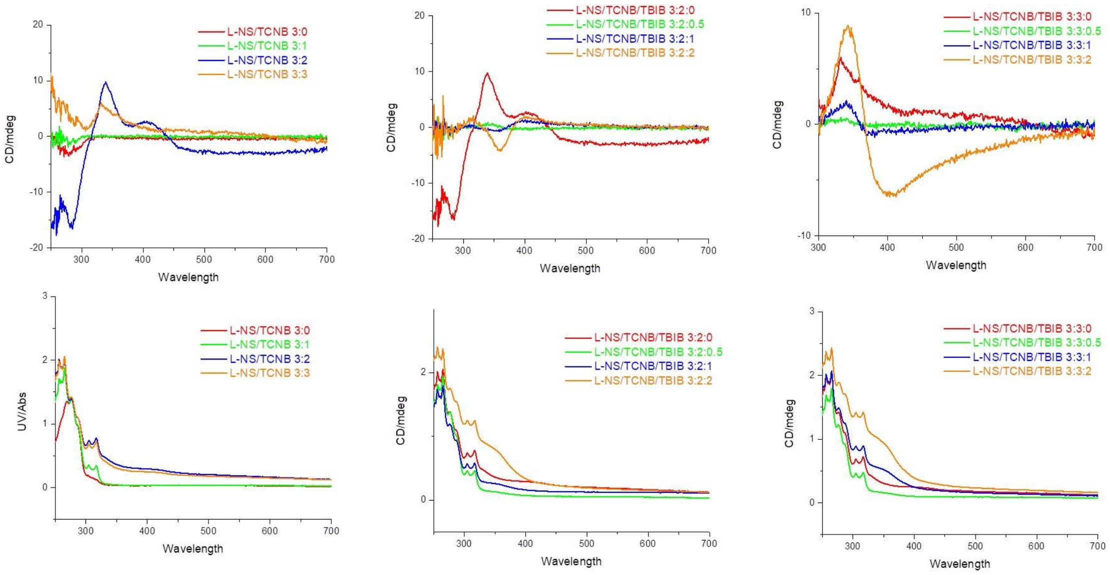

Fig. S1 CD and absorption spectra of different NS coassemblies, which were carried out in solution phases. Self-assembled dispersions were vortexed before characterization.

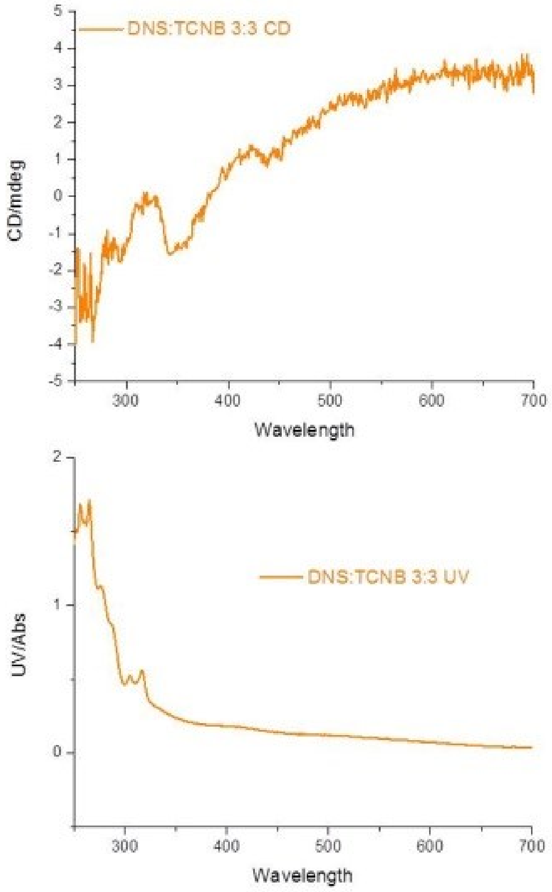

Fig. S2 CD and absorption spectra of D-NS/TCNB coassembly, which were carried out in solution phases. Self-assembled dispersions were vortexed before characterization.

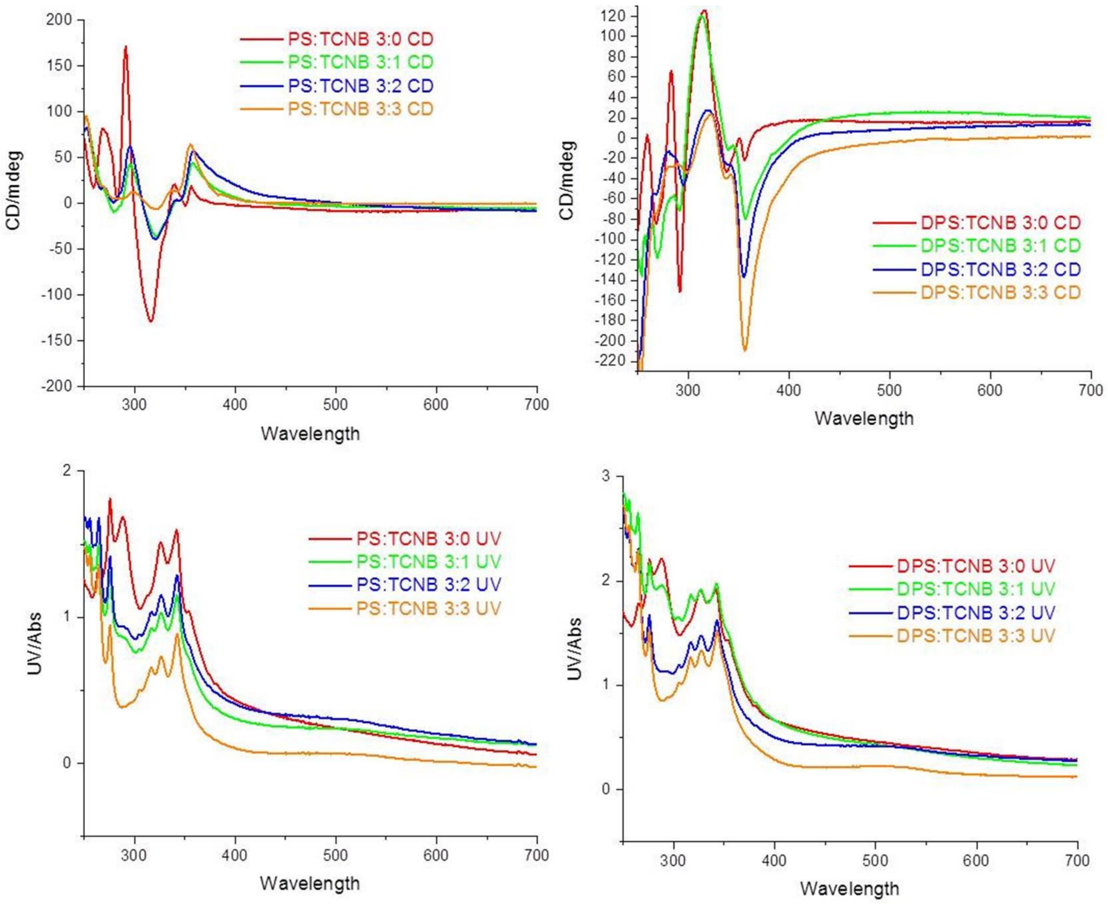

Fig. S3 CD and absorption spectra of L-PS/TCNB and D-PS/TCNB coassemblies with different molar equiv. of TCNB, which were carried out in solution phases. Self-assembled dispersions were vortexed before characterization.

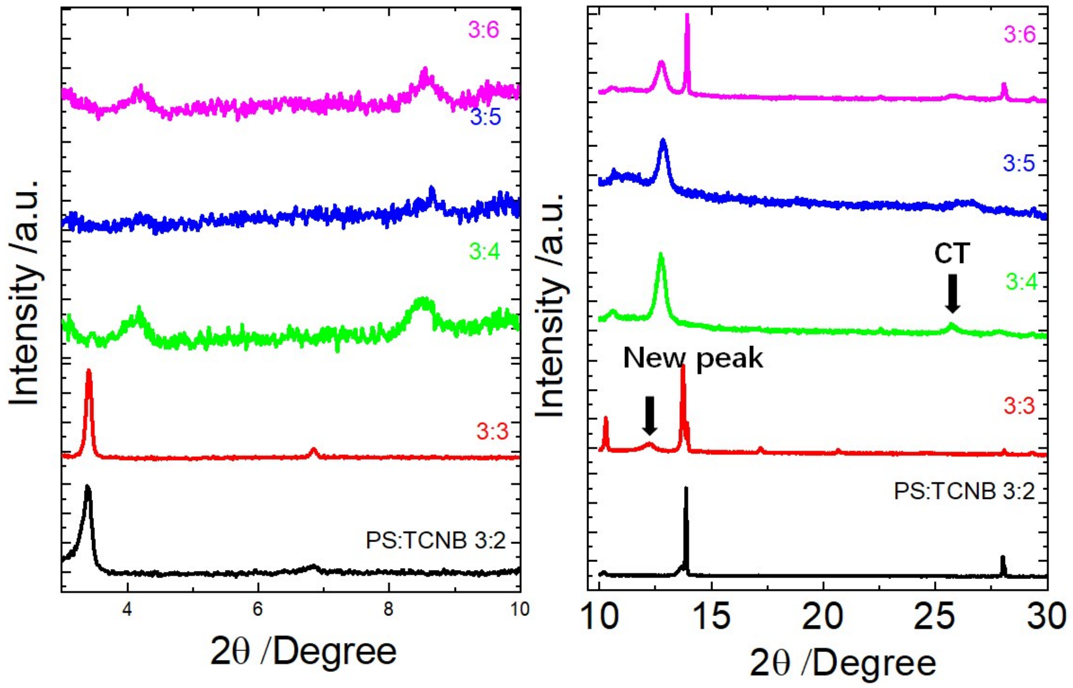

Fig. S4 XRD patterns of L-SP:TCNB coassembly with different TCNB molar equiv.

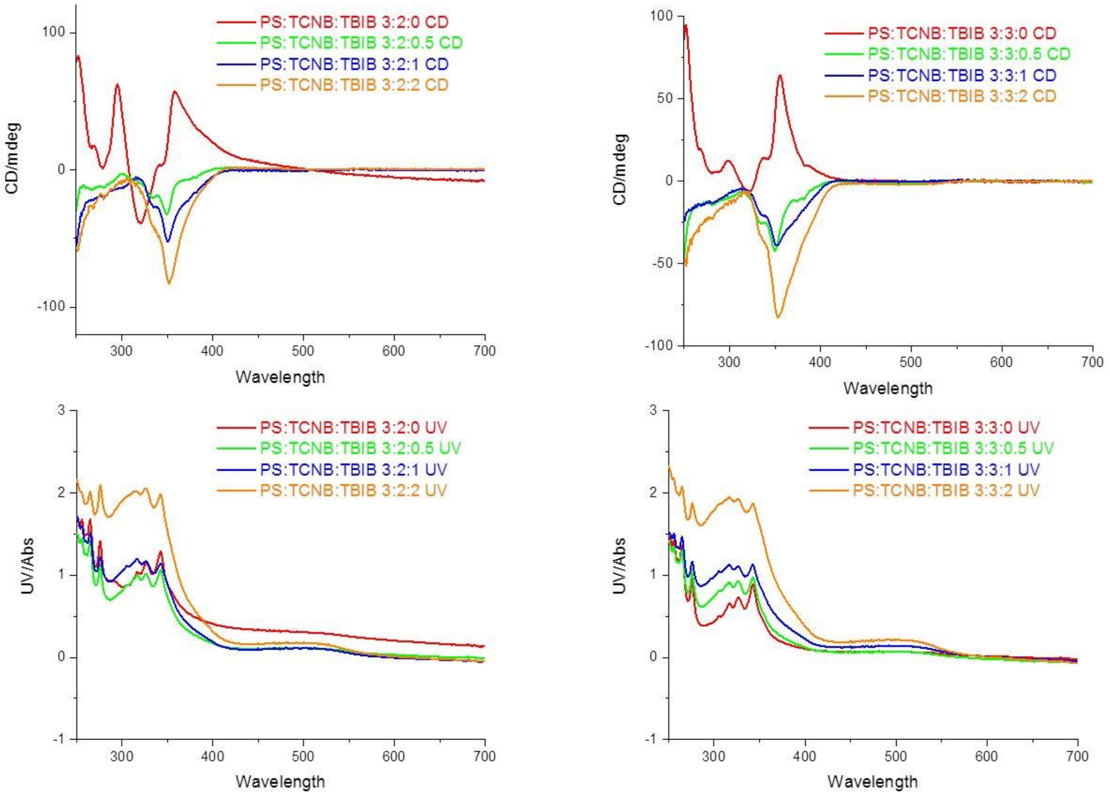

Fig. S5 CD and absorption spectra of L-PS ternary coassembly with different TBIB molar equiv., which were carried out in solution phases. Self-assembled dispersions were vortexed before characterization.

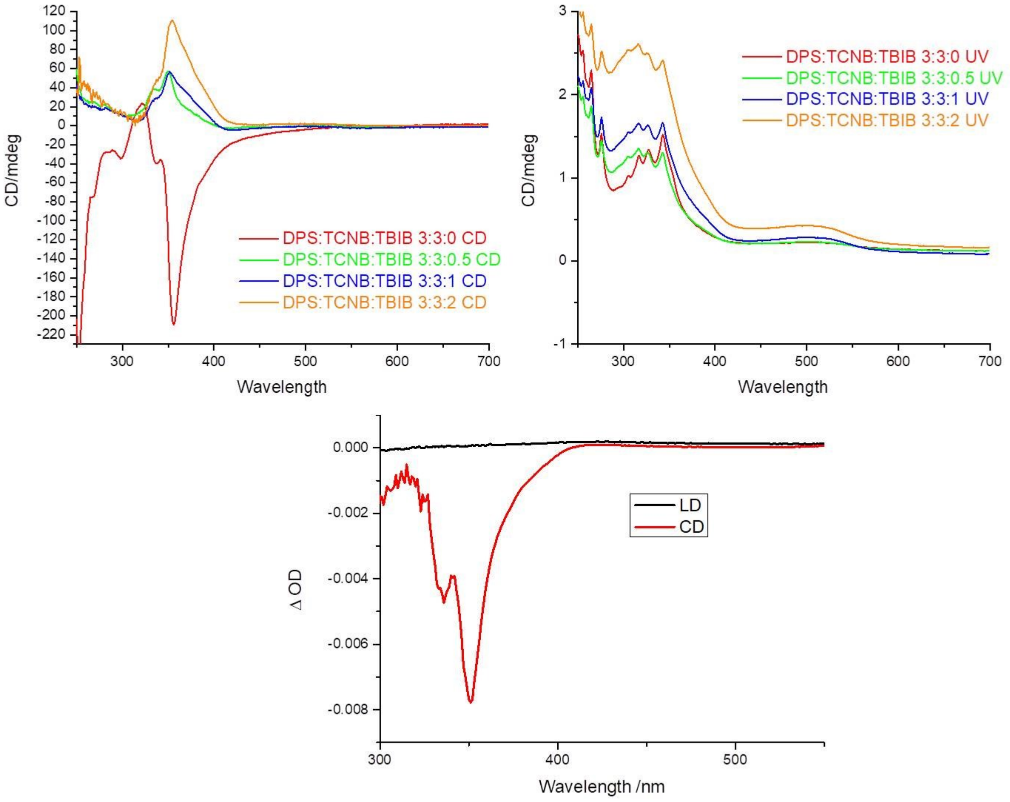

Fig. S6 CD and absorption spectra of D-PS ternary coassembly with different TBIB molar equiv. Below image is LD spectrum of PS ternary coassembly (L-PS:TCNB:TBIB 3:3:1). Samples were carried out in solution phases. Self-assembled dispersions were vortexed before characterization.

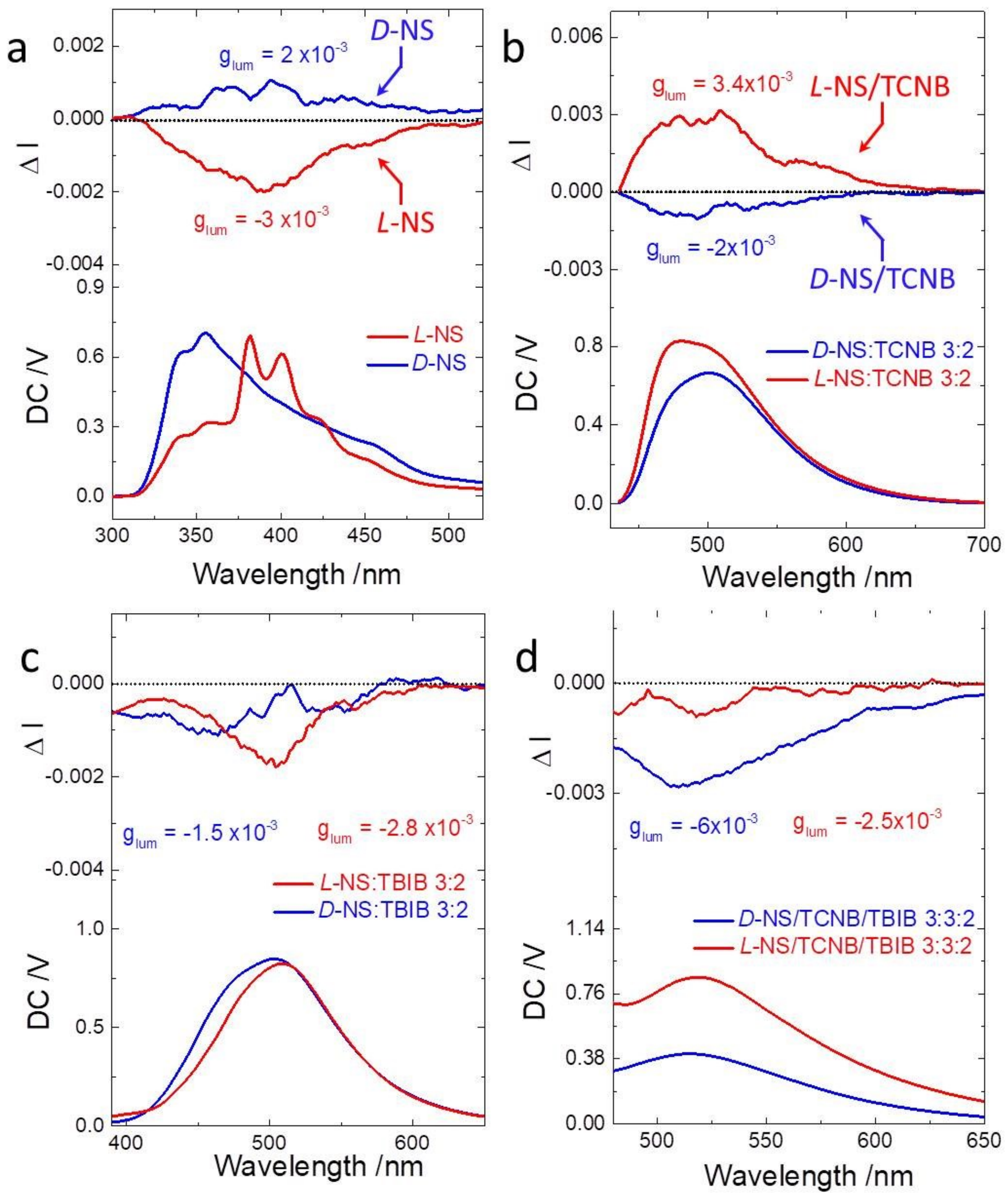

Fig. S7 CPL spectra of NS coassemblies excitated at 280 nm, 420 nm, 350 nm, 520 nm, respectively. It is worth noting that the DC spectra of NS-isomers are different. We calculated the HOMO-LUMO gap of different species at the B3LYP/6-31G (d) level with Gaussian 16 program. HOMO-LUMO gap values of L-NS, D-NS, L-PS and D-PS are 4.6937, 4.8387, 3.7893 and 3.7898 eV respectively. It suggests that the deviations between D/L-NS and D/L-PS are 0.145 and 0.0005 eV respectively. The separation of 0.145 eV corresponds to a emission shift about 60-70 nm, which is in good agreement with the emission shift observation

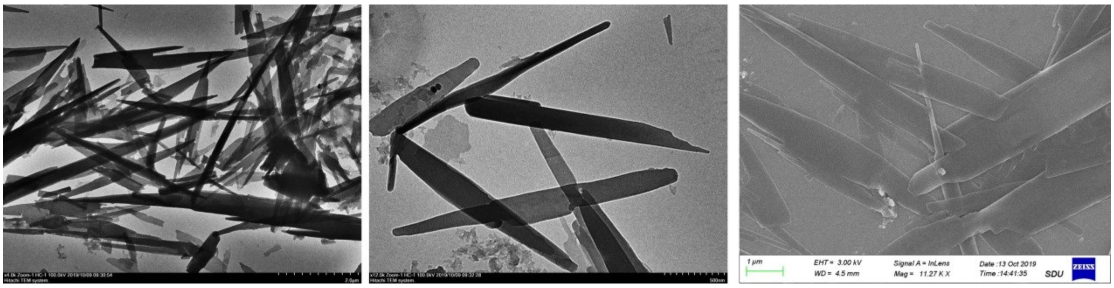

Fig. S8 TEM and SEM images of binary L-NS/TCNB 3:3 coassemblies.

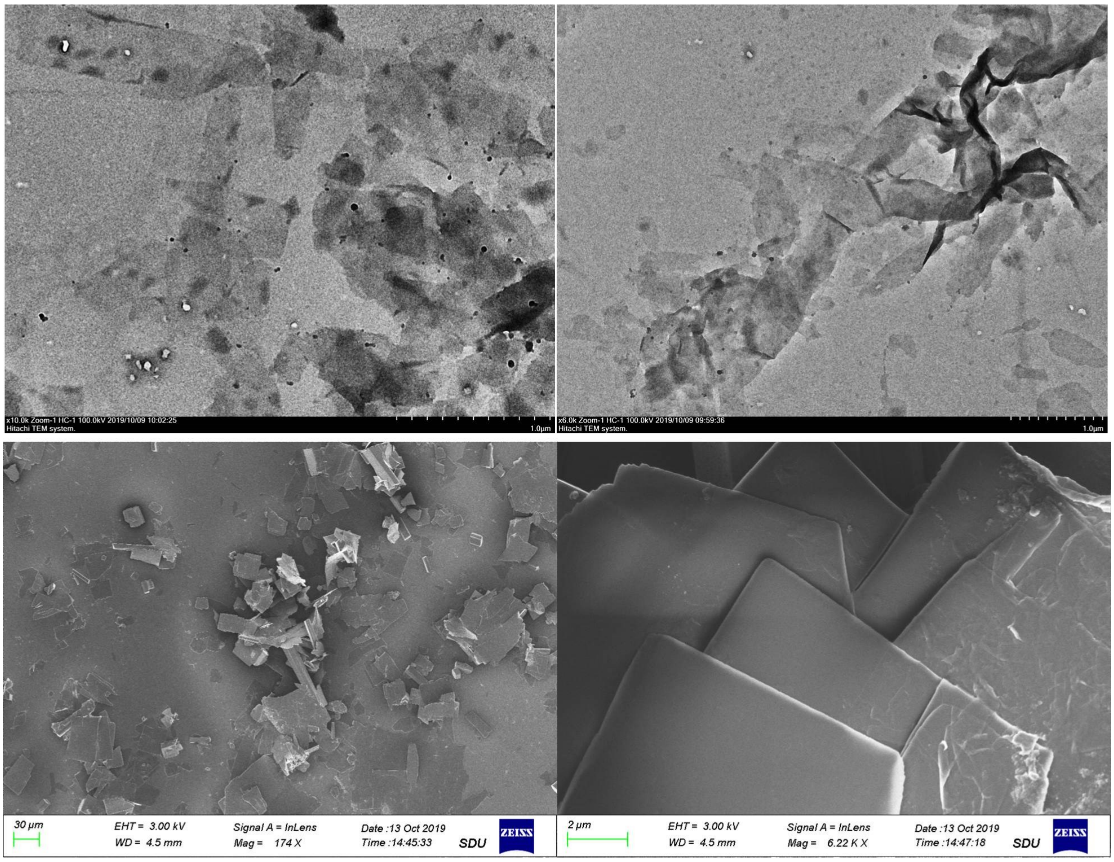

Fig. S9 TEM and SEM images of binary L-PS/TCNB 3:3 coassemblies.

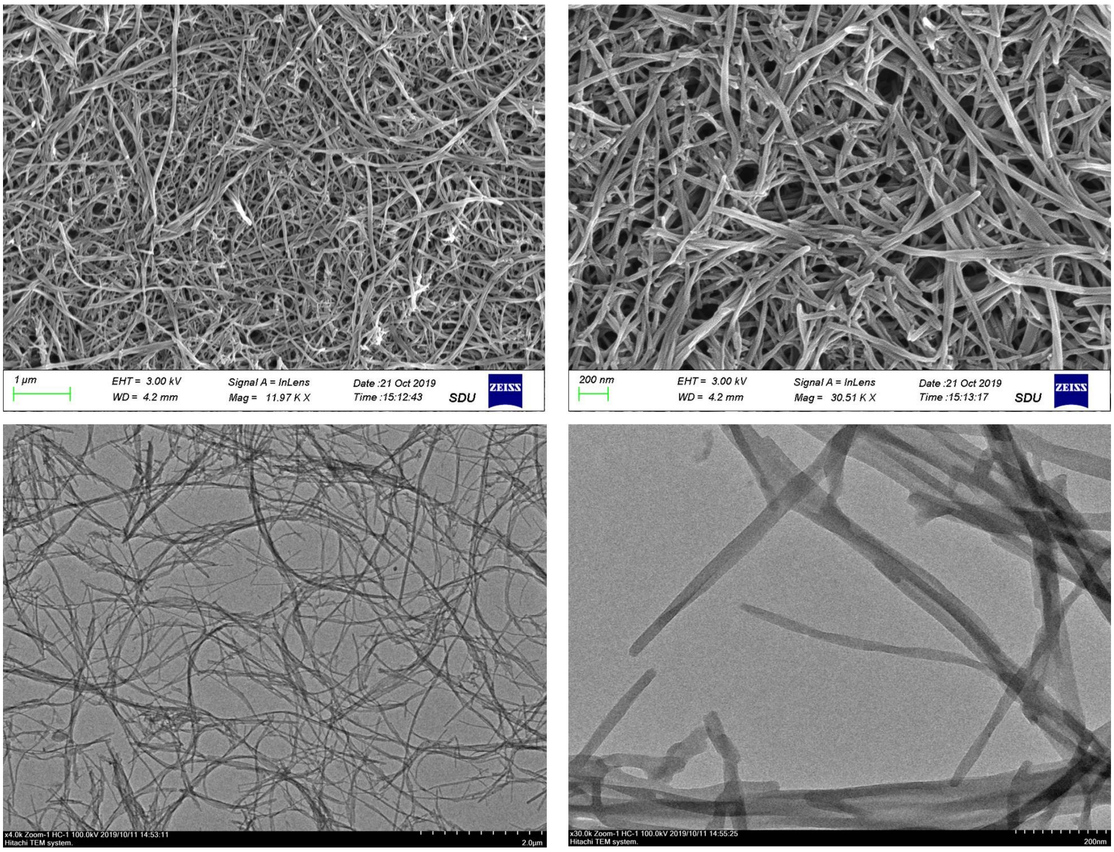

Fig. S10 SEM and TEM images of L-NS/TCNB/TBIB (3:3:1) ternary coassemblies.

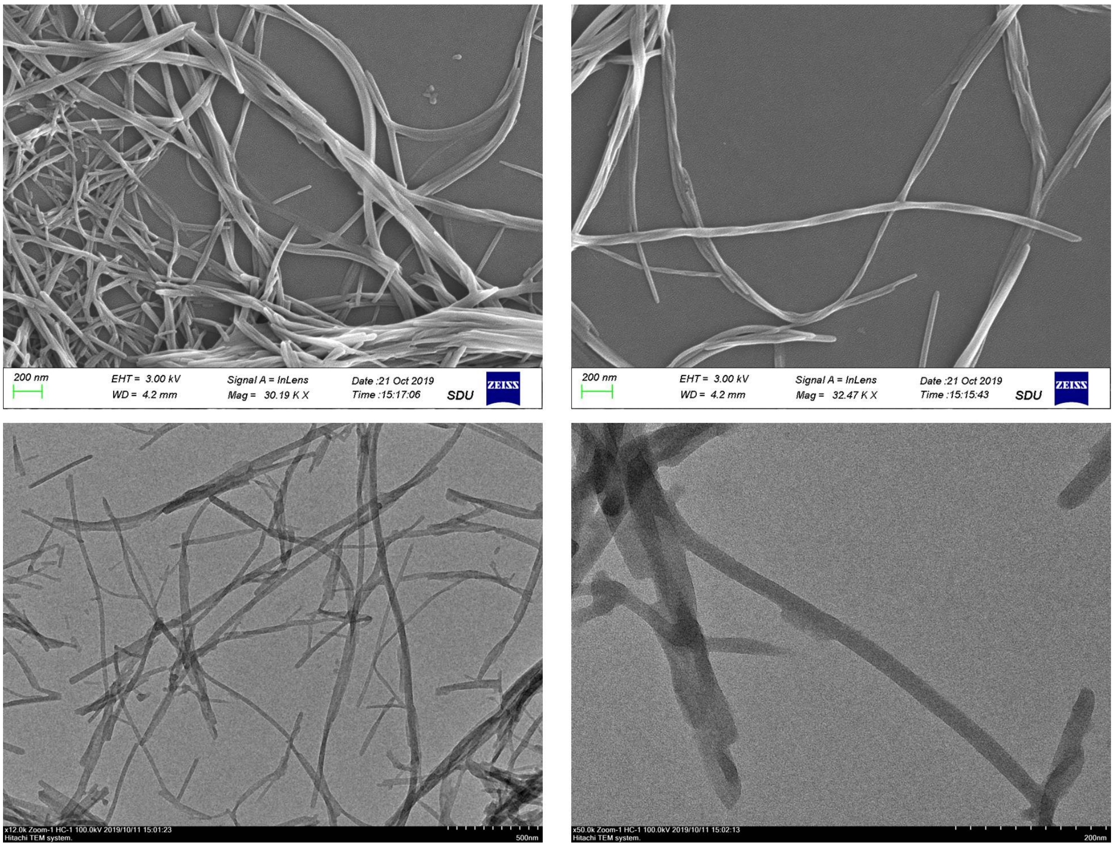

Fig. S11 SEM and TEM images of L-NS/TCNB/TBIB (3:3:2) ternary coassemblies.

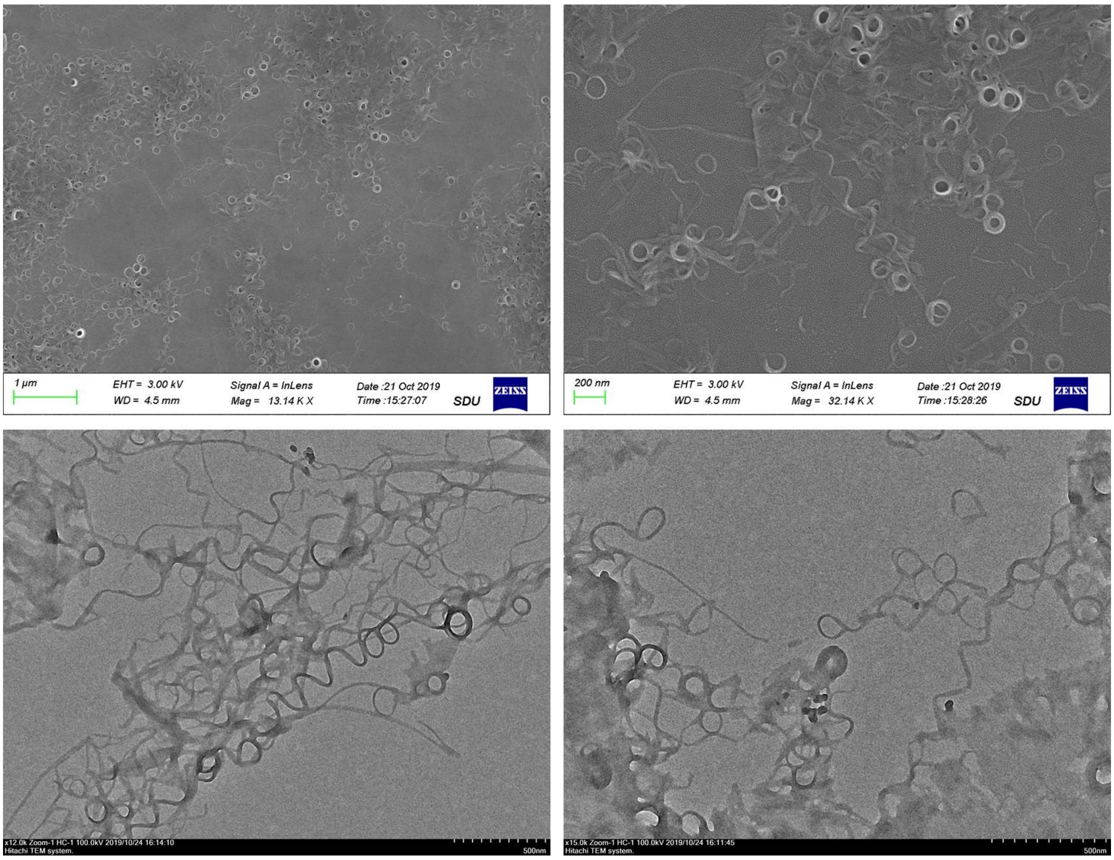

Fig. S12 SEM and TEM images of L-PS/TCNB/TBIB (3:3:1) ternary coassemblies.

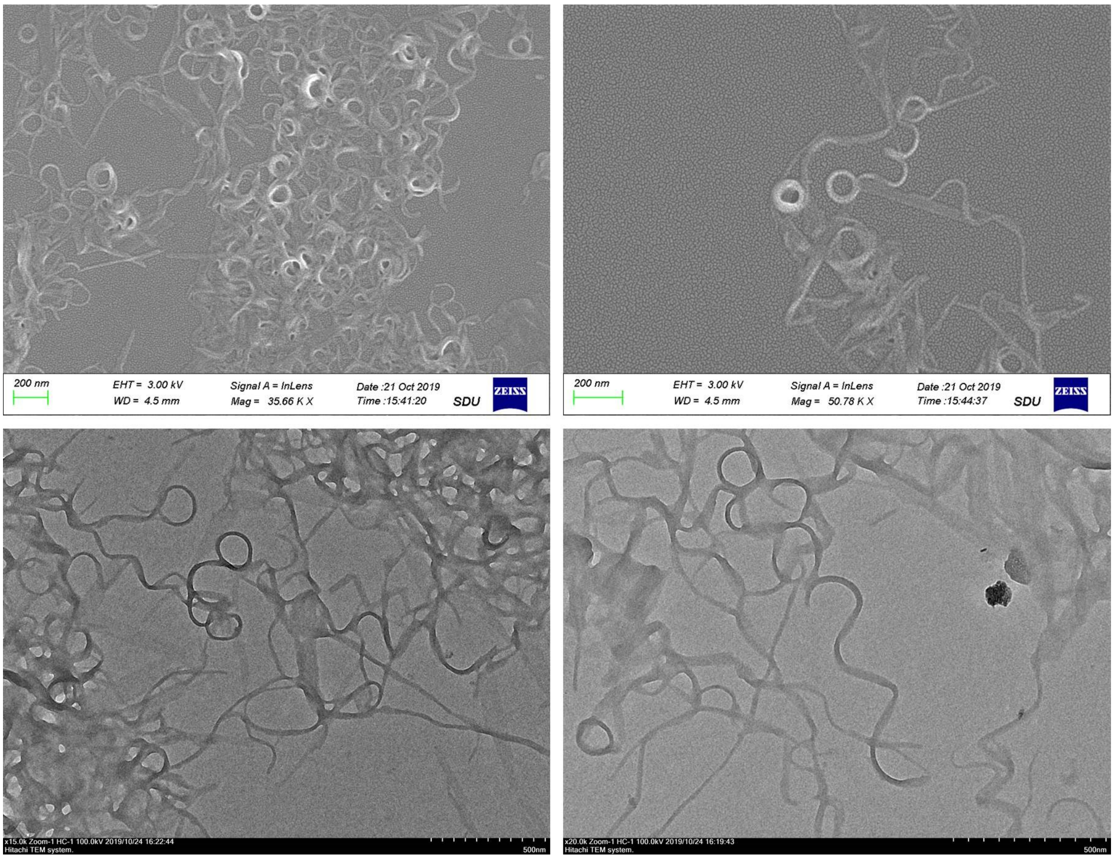

Fig. S13 SEM TEM images of L-PS/TCNB/TBIB (3:3:2) ternary coassemblies.

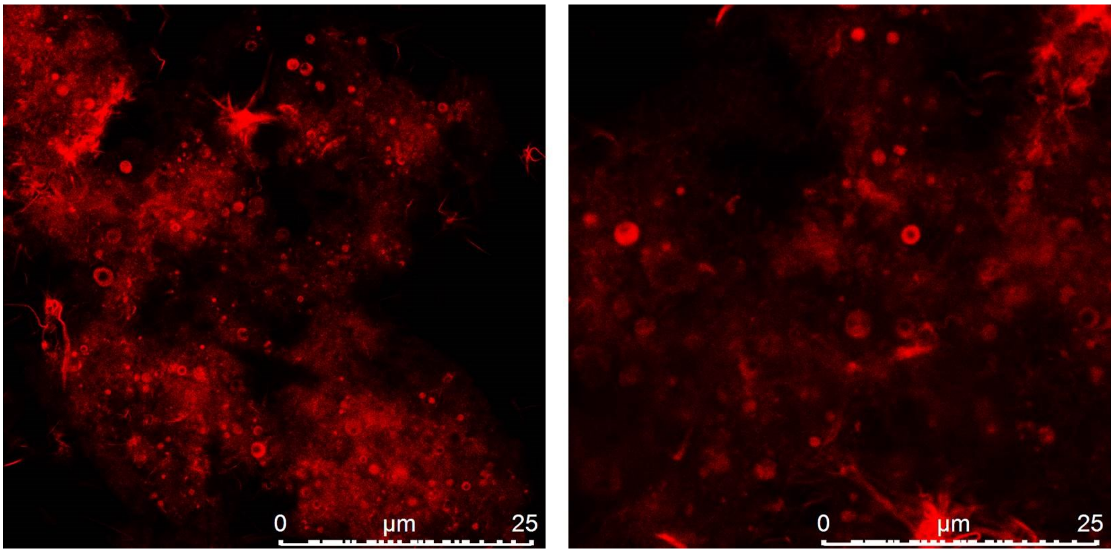

Fig. S14 CLSM images of PS (3:3:1) ternary coassemblies.

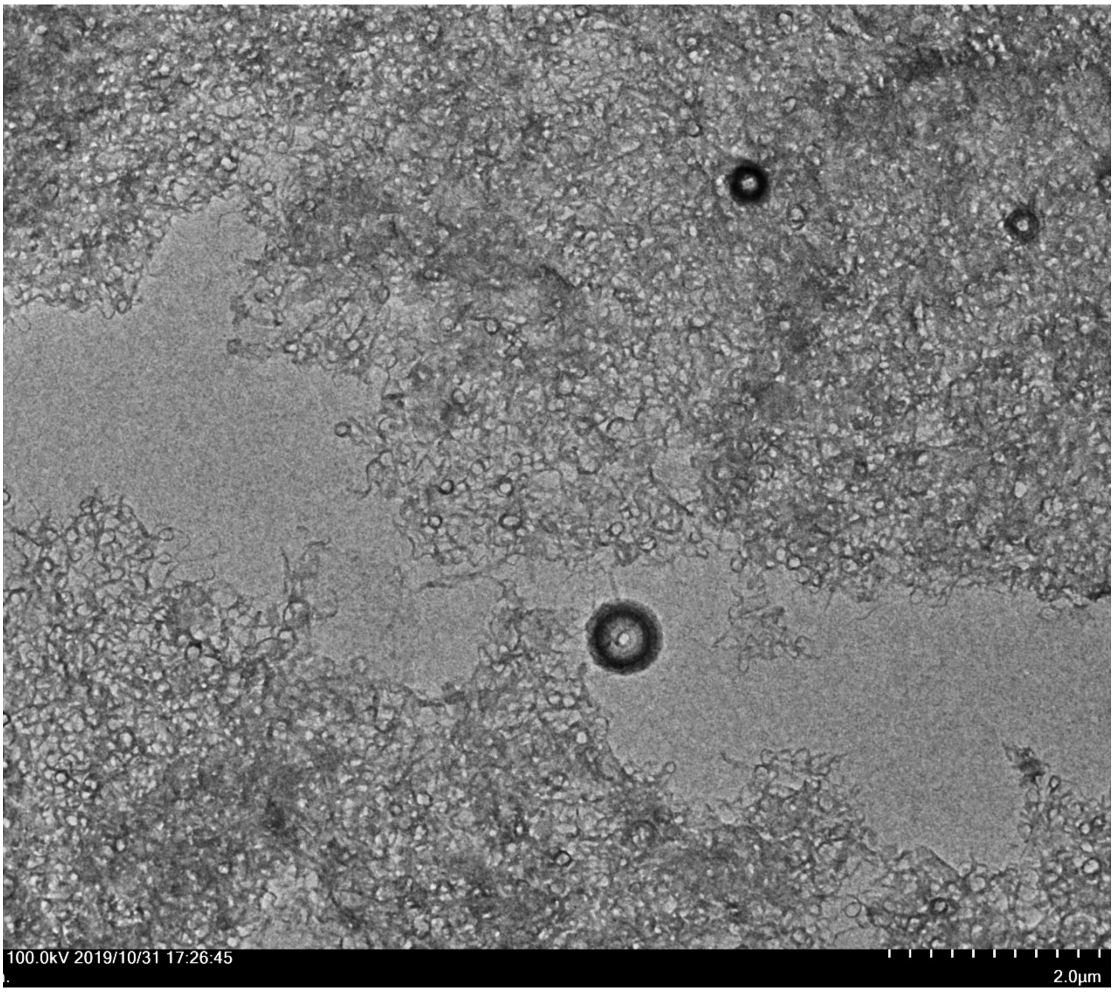

Fig. S15 TEM image of PS ternary coassembly (3:3:2) with giant toroidal structure.

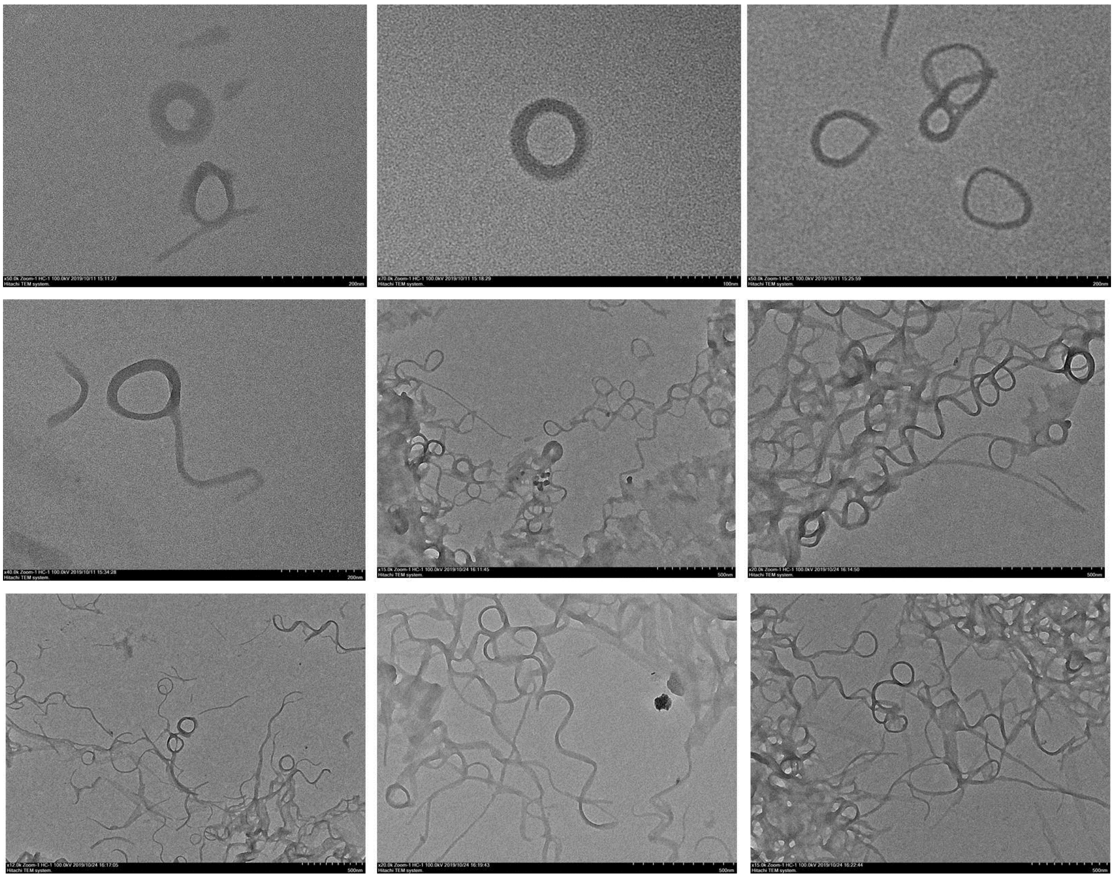

Fig. S16 Additional TEM images of toroidal structures and superstructures from PS ternary coassembly (3:3:1 and 3:3:2)

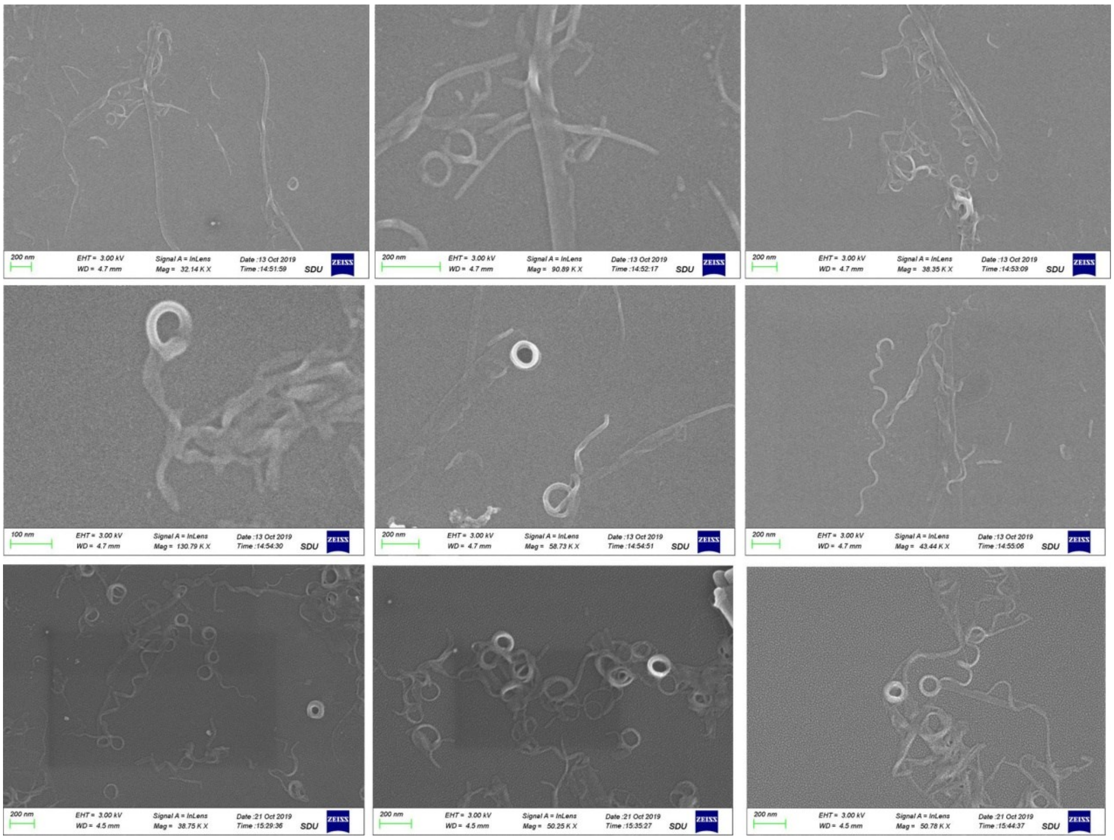

Fig. S17 Additional SEM images of toroidal structures and superstructures from PS ternary coassembly (3:3:1 and 3:3:2)

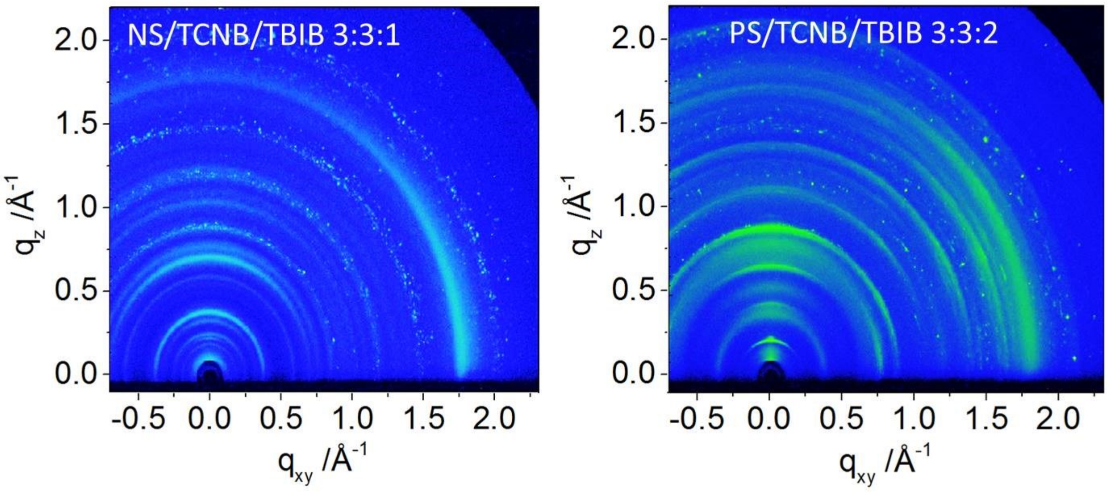

Fig. S18 GiSWAXS patterns of ternary coassembly

References

S1. Xing, P.; Li, Y.; Xue, S.; Phua, S. Z. F.; Ding, C.; Chen, H,; Zhao, Y. Occurrence of Chiral Nanostructures Induced by Multiple Hydrogen Bonds. *J. Am. Chem. Soc*., **2019**, *141*, 9946-9954